COBEM 2023 27TH INTERNATIONAL CONGRESS OF MECHANICAL ENGENEERING

ABCM Brazilian Society of Mechanical Sciences and Engineering
27th ABCM International Congress of Mechanical Engineering
December 04-08, 2023, Florianópolis-SC, Brazil

COB-2023-1885
Design and Performance Optimization of Scaled Rotary Blades for Additive Manufacturing

Giulia Derneka Maccarone
derneka.maccarone@unesp.br
Murilo Sartorato
murilo.sartorato@unesp.br

Daniel Sampaio Souza
daniel.s.souza@unesp.br

Marcelo Jorge Filho
marcelo.jorge@unesp.br

Carlos do Carmo Pagani Júnior
c.pagani@unesp.br

São Paulo State University (UNESP). Campus of São João da Boa Vista. Av. Profa. Isette Correa Fontão, 505 - Jardim das Flores, São João da Boa Vista - SP, 13876-750.

Abstract. *This study reports on the methodology and results of an ongoing study focused on the parametric optimization of both aerodynamic and structural performance of subscale rotary wings operating at low Reynold hovering flight. The rotary wings engineering project relies on the integration between an aerodynamic numerical model and manufacturing processes based on additive manufacturing techniques. An in-house code based on the Blade Element Momentum Theory (BEMT) is applied to simulate the induced flow field, aerodynamic loading and rotor performance within a range of design parameters and operational conditions typical of unmanned aerial vehicles (UAV). The rotor aerodynamic performance is quantified based on the rotor solidity, airfoil geometry, wing taper ratio, thickness, camber and spanwise twist ratio. A conceptual blade design is developed by using the software Fusion 360 and built with a 3D printer through the Fused Deposition Modeling (FDM) additive manufacturing process. However, the use of additive manufacturing processes to design and building aeronautical devices, notably rotary wings, has been seldom reported in the literature, and optimizing processes can lead to a challenging design from the structural and aerodynamic points of view. This research is motivated by the increasing tendency in the use of small vehicles based on fixed or rotary wings for civilian, agricultural and military applications, and justified by the necessity of better understanding the behavior of scaled models and the application of modern prototyping tools in the laboratorial level and also driving basic and applied researches towards technological innovations, leading to new generations of small scale aircrafts able to overcome the current technical limitations and to attend the increasingly environmental requirements.*

Keywords: *Rotary wings, aerodynamic performance, rotors design, parametric optimization, additive manufacturing*

1. INTRODUCTION

The increasing use of unmanned aerial vehicles for both civilian and military purposes, as well as small and lightweight aircrafts designed for a small number of passengers, less than a dozen, poses several technological challenges for the scientific community. Such subscale vehicles commonly use rotary wings for lifting and propulsion operating at low Reynolds number regimes (Valavanis and Vachtsevanos, 2014) (Muller and Delaurier, 2003).

The current requirement for the development of high-efficiency competitive vehicles based on sustainable technologies opens room for optimizing rotor design, which can lead to better structural performance, improve aeroelastic stability and reduce noise emission. In view of that, the development of rotary wing experimental bench tests creates the possibility to conciliate basic research and technological innovation based on a multidisciplinary approach. A high-efficiency rotor design requires the optimization of blade geometry parameters and airfoil section for operation at a particular Reynolds number regime (Bohorquez *et al.*, 2010); in addition, efforts have been devoted to combining the structural and aerodynamic optimization process with flow analysis techniques for helicopter rotors (Sun and Lee, 2005) and wind turbines (Clausen *et al.*, 2023).

This paper reports an ongoing study to support the engineering design of a scaled rotary blade prototype to study the

aerodynamic and aeroelastic behavior at operational conditions corresponding to low Reynolds number hovering flights. Numerical simulations with a scaled laborational rotor at low Reynolds number was performed by using Blade Element Momentum Theory (BEMT) (Leishman, 2006) (Seddon and Newman, 2011) to investigate the effects of blade geometry on the rotor aerodynamic efficiency.

The blade conceptual design was developed to achieve the nominal aerodynamic performance predicted from a parametric study accomplished with an in-house code based on Blade Element Momentum Theory. The NACA-4412 airfoil, reported in a benchmark aeroacoustic study for low Reynolds number propeller (Casalino *et al.*, 2021), was selected. The non-dimensionalized lift and drag aerodynamic coefficients for the selected airfoil were obtained within a range of angles of attack and Reynolds number of interest by using the XFOIL software. Once the airfoil geometry was selected, taper ratio and twist rate are added to the three-dimensional blade by extruding the 2D wing section. A computational code based on the Blade Element Momentum with a lookup table strategy and data interpolation was used to calculate the lift and drag forces at each blade section from the XFOIL database.

Mechanical behavior, material strength, dimensional tolerance and surface finish resulting from the additive manufacturing process must be carefully assessed to assure a high-quality blade prototype for reliable bench tests. The software Fusion 360 was applied as a computer aided design tool to develop the blade conceptual design and, as a future work, perform static and dynamic structural analysis. The first conceptual blade design prototype was built by a 3D printer through the Fused Deposition Modeling (FDM), which is an additive manufacturing process based on material extrusion (Schiller, 2015). By this technique, the prototype is built layer by layer by the deposition of melt material (polylactic acid was used).

As such, the result of building a blade prototype is presented and some relevant aspects of the manufacturing process are discussed. A rotary wing numerical model sharing the tapered and twisted features of the manufactured subscale blade prototype was implemented and aerodynamically simulated with a computational code based on the Blade Element Momentum formulation. Results of a preliminary parametric study to quantify the rotor aerodynamic performance based on blade design parameters at prescribed operational conditions are presented. The numerical results were consistent with regards to the role played by the wing geometry on the flow field and rotor performance. From that, the structural and manufacturing limit to apply optimal design parameters in building subscale rotary blades based on optimization processes can be further investigated.

2. Theoretical Foundation and Research Methodology

2.1 Numerical Simulations Based on the Blade Element Momentum Theory

The Blade Element Momentum Theory (BEMT) is mainly used to analyze the performance of rotary wings, such as those found in helicopters and wind turbine blades. It divides these blades into small sections and considers the local angle of attack constant for each section (element theory). BEMT then employs principles of mass and momentum conservation (momentum theory) to numerically predict the spanwise distribution of both induced flow velocity and angle of attack based on the blades geometry and the rotor operational conditions; and from these the spanwise distribution of aerodynamic efforts (lift, drag and pitch moment) on each element and the resulting forces and moments on the entire system and, therefore, the overall rotor loading, aerodynamic performance, thrust, power output, and efficiency.

A rotor performance is dependent on the blade section geometry (airfoil) and design parameters, such as solidity, taper ratio and root-to-tip twist rate. Most small-sized flying vehicles, including micro air vehicles and eVTOLs, operate at low Reynolds numbers based on the wing chord and, therefore, undergo power loss due to higher induced drag also associated with the occurrence of laminar separation bubbles. At hover flight the rotor performance can be quantified based on an efficiency parameter named Figure of Merit, which takes into account both effects from induced and profile drag components.

An ideal rotor, which operates without any energy loss, would reach a Figure of Merit equal to 1, whereas real rotors, in turn, have a Figure of Merit smaller than 1. High efficiency rotors may achieve Figure of Merit of about 80%, meaning that up to 20% of the total power received by the rotor is lost. Due to the Figure of Merit dependence on the thrust coefficient, rotors performances should be compared with the same disk loading in order to identify the net effect of each design parameter on the rotor efficiency. For numerical simulations, we consider the variation of solidity due to the tapered-blade planforms, so that most performance results are presented based on the blade-loading coefficient C_T/σ.

The blade collective pitch angle can be set in order to assure that rotors with different design parameters operate at the same disk loading, which is accomplished by iteratively running the Blade Element Momentum computational code until the convergence of the collective pitch angle is achieved for the rotor configuration at a given operational condition (Leishman, 2006). Lift and drag coefficients for the NACA-4412 airfoil were calculated by using the XFOil software.

2.2 Rotor Design Performance

Rotor performance optimization enables to reduce the power plant requiriment to improve the flight range and endurance of aerial vehicles based on rotary wings. This section addresses the role played by the blade design on the rotor efficiency and power requirement. From the Blade Element Momentum Theory, rotor thrust, T, and power, P, are respectively given by

$$T = C_T \rho A \left(\Omega R\right)^2, \tag{1}$$

and

$$P = C_P \rho A \left(\Omega R\right)^3, \tag{2}$$

where C_T and C_P are the nondimensional thrust and power coefficients, and A is the rotor area. The ratio between thrust and power can be written as

$$\frac{T^3}{P^2} = \frac{C_T^3}{C_P^2}\rho A, \tag{3}$$

from which the power is given by:

$$P = \frac{T^{3/2}}{R\sqrt{\rho\pi}\frac{C_T^{3/2}}{C_P}}. \tag{4}$$

The Figure of Merit is related with thrust and power coefficients as follows (Leishman, 2006)

$$FM = \frac{C_T^{3/2}}{\sqrt{2}C_P}. \tag{5}$$

From Equations 4 and 5, we state the rotor power dependence on both Figure of Merit and mechanical efficiency coefficients, η:

$$P = \frac{T^{3/2}}{R\sqrt{2\rho\pi}}\left(\frac{1}{\eta FM}\right). \tag{6}$$

Whether it is required, the thrust on the rotor is steemed from Eq. 6 according to

$$T = \left(\eta P R\sqrt{2\rho\pi}FM\right)^{2/3}. \tag{7}$$

Equation 6 allows to predict the power requirement for rotors designed at the same disk loading and will be used here to quantify rotor performances based on the blade geometry and design parameters.

3. Rotary Blade Design For Additive Manufacturing

3.1 Wing Cross Section Geometry and Design

Tha NACA-4412 airfoil has been selected for this study. It is an asymmetric airfoil, which generates lift even at zero angle of attack, with maximum thickness of 12% at 30% chord and maximum camber of 12% at 40% chord. The wing cross section was conceived to resemble that of a real wing while being simple enough to be customizable and easily manufactured through additive manufacturing, i.e. having a simple enough structural design with no hanging parts, and no sudden changes of angles, to allow for the extrusion process of a solid with thin walls. For that the authors aimed for a torque box strucutre with two spars located in typical positions of 15% and 70% of the chord, the upper and lower surfacs manufatured with the smallest thickness possible given the available equipment and the spars manufactured with triple walls. The upper surface included three rectangular reinforcement beams (stringers) to increase the equivalent torsion stiffness of the system.

3.2 Pretwisted Blade Design

The geometric torsion of the blade was set at -8°, with the torsion centered in a point resting on structure shear center; the shear center was calculated by ANSYS SpaceClaim as a position of (390, 42) mm away from the leading edge. The final crossection drawing of the root and tip of the blade superimposed are shown in Figure 1. The outer sections were connected though a linear interpolation using a loft operation on SpaceClaim guaranteeing a linear distribution on torsion angle, and straight leading and trailing edge. The spars were made by filling the interssection of the created outer skin with vertical planes positioned on the aforementioned positions. Figure 1 shows a blade section shaped with airfoil NACA-4412. The relative rotation between the root and tip sections represents the geometric effect of twisting the blade by -8° using the software Fusion 360.

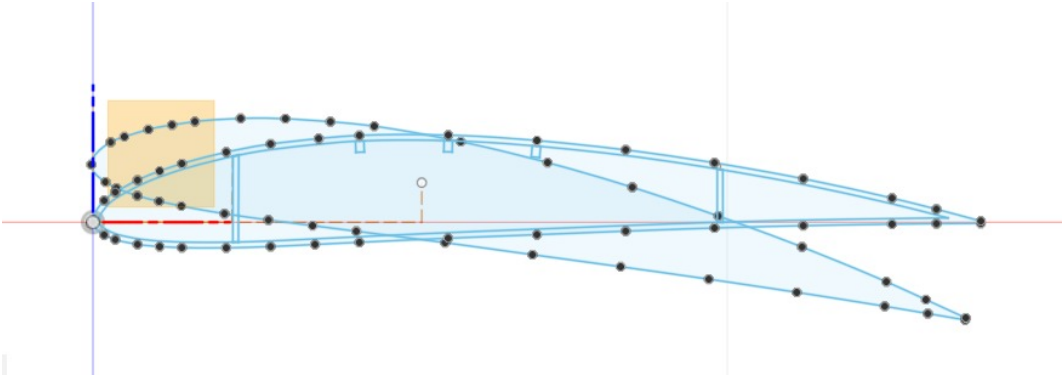

Figure 1. Root and tip cross sections showig a geometric twist angle of -8°.

3.3 Additive Manufacturing

There are several additive manufacturing processes, most of them based on building parts in layers, the main difference being how they make this construction; which can be separated into: liquid-based rapid prototyping, powder bed fusion process, and solid based rapid prototyping. Rapid prototyping has experienced explosive growth in recent years, primarily driven by the compelling demand among engineers, designers and researchers for tangible physical models, as opposed to relying solely on computational representations. This surge can be attributed to the necessity for conducting tests and experiments that require a hands-on approach. In the aeronautical and aerospace industries, a 3D printed part can be tested in a wind tunnel, allowing the aerodynamic characteristics to be obtained as well as the stability and structural characteristics to be studied.

3.3.1 Fused Deposition Modeling

This rapid prototyping method is an extrusion based system and one of the most employed additive manufacturing systems; it uses a heating chamber to liquify a filament of polymer at a precise temperature, strategically set just above the polymer's melting point. For the present work, the chosen filament material is chosen as polylactic acid (PLA), a polymer known for its capability of fast biodegradation and low cost of production, making the final product available for industrial use. Its main disadvantage is that as the filament is extruded by a circular nozzle it is difficult to create geometries sharper or thinner than the nozzle's diameter. For the present work this could interfere with some parts of the model such as the trailing edge, which is intended to be as thin as possible.

Another problem is found in the layer height, which is fixed by the filament and printer characteristics; when excessively thick layers are utilized, it can lead to not only inefficiencies but also failure in the manufacturing process, creating faulty parts with holes or distorted shapes. Also, the layer thickness influences the roughness of the surface, influencing the way the airfoil interacts with the air flow. As shown in Figure 2, the larger layer thickness led to a larger roughness coefficient, making the layer separation more visible when sliced and printed.

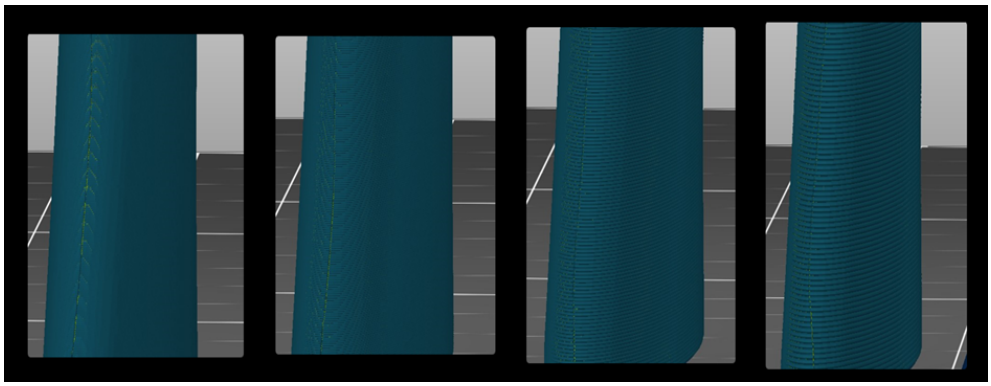

Figure 2. Influence of layer thickess on the surface roughness for layer height: 0,05mm ; 0,012mm ; 0,02mm ; 0,032mm

3.4 Prototpe design

Initially the wing internal structure was designed by simply using the slicer filing using a grid of angled walls without any reinforcement by using an extrude operation in the Fusion 360 software and choosing the filling percentage (15%)

in the PrusaSlicer software. In order to make the project more realistic to what a typical semi-monocoque wing structure geometry is and behaves as, to minimize material waste, and guarantee a finer structure the grid filling was replaced with reinforcement walls as seen in Figure 3.

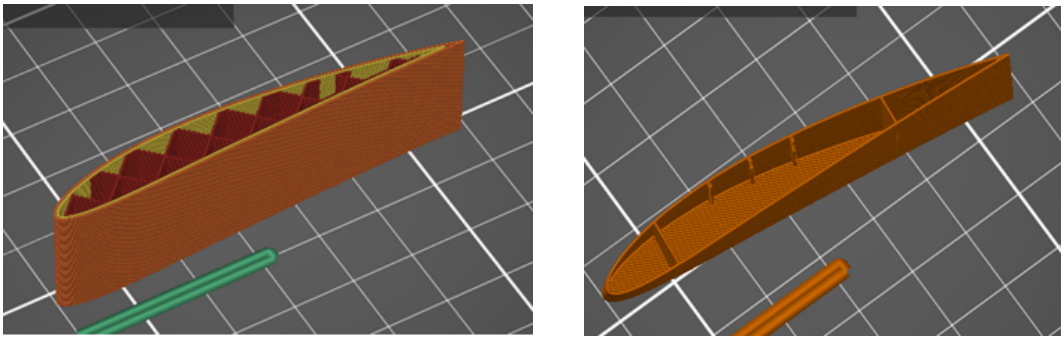

(a) (b)

Figure 3. Inital fillig and semi-monocoque proxy philosophy

Some problems were found in the printing process, the airfoil needs at least three perimeter walls because of the way the printer makes a deposition entrance on the reinforcements marking the outside part of the airfoil, adding walls is an advantage when it comes to the reinforcement being thicker, adding value to the structure's strength. Figure 4 shows a finalized prototype, with proper application of torsion: the linear distribution of the geometric torsion angle through the span of the wing is visualized as straight lines along the leading and trailing edges.

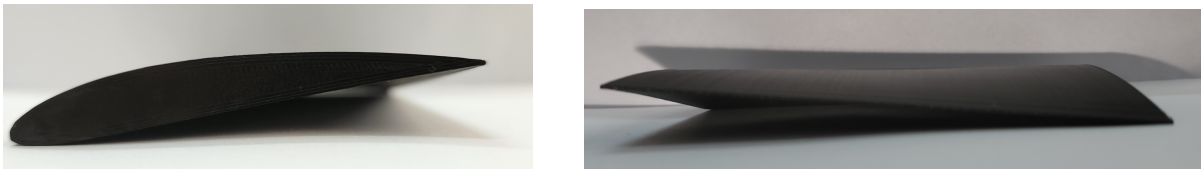

(a) (b)

Figure 4. Front and side views of the prototype showing the airfoil and the trailing edge

3.5 Tapered Blade Design

A tapered blade is one for which the chord length (and therefore the local rotor solidity) varies from the root to the tip. The taper ratio is defined as the ratio between the chord lengths measured at the blade ends. For instance, the notation 3:1 means that the chord length reduces in the ratio of 3 to 1 from the root to the tip. Although a linear variation is commonly assumed, more complex blade geometries have been reported in the literature (Casalino *et al.*, 2021) (Loureiro *et al.*, 2021).

Blade tapering based on the thrust-weighted solidity was adopted in this research, which allows to find the equivalent solidity of a rectangular blade that produces the same lift as a linearly tapered one with a prescribed taper ratio. For a spanwise constant mean lift coefficient, it turns out that a rectangular blade solidity matches the local solidity of a linearly-tapered blade at $\bar{r} = 0.75$, with $\bar{r}$ being the nondimensional spanwise position (Leishman, 2006).

Figure 5 shows the chord length radial distribution of blades with taper ratio of 1:1, 2:1 and 3:1, obtained from a two-bladed rotor with weighted solidity of 0.1536, as stated in Table 1. According to Figure 3(b), the chord length of a constant solidity rotor increases at the blade root whereas decreases at the blade tip as the taper ratio increases, so that the chords (and therefore the local solidities) match the equivalent balde chord at a 75% spanwise, as required to achieve a thrust-weighted solidity.

Results from numerical simulations of rotary taper blade with the method Blade Element Momentum are presented in (Boni *et al.*, 2021). The approach, which is applied in this study, consists in applying the concept of thrust-weighted solidity to find the spanwise chord distribution of a linearly-tapered blade that produces lift as a reference rectangular blade with a prescribed chord or solidity. Equation 8 (reproduced from (Boni *et al.*, 2021)) shows the local solidity, $\sigma\left(\bar{r}\right)$, as a function of the nondimensional spanwise position, $\bar{r}$,

$$\sigma\left(\bar{r}\right) = \frac{\left(1-\gamma\right)\bar{r}+\gamma}{\left(1-\gamma\right)0,75+\gamma}\sigma_e. \tag{8}$$

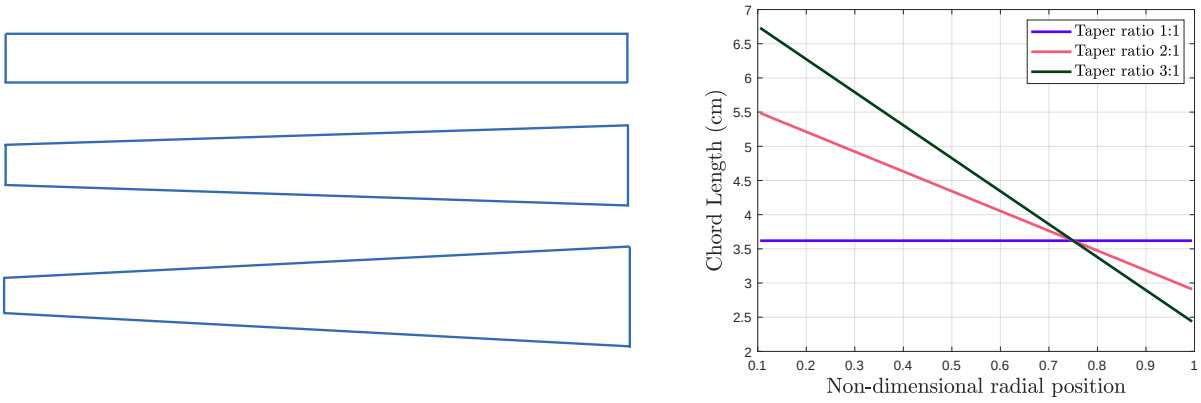

(a) (b)

Figure 5. Figura 5(a): planar surfaces of thrust-weighted blades with taper ratios of 1:1, 2:1 e 3:1. Figura 5(b): chord length radial distributions of thrust-weighted blades with taper ratios of 1:1, 2:1 e 3:1.

In Equation 8, γ represents a numerical entry parameter to the selected taper ratio ($\gamma = 3$ for taper ratio of 3:1, for instance), and σ_e is the equivalent solidity of reference blade.

3.6 Rotor Design

The aerodynamic efficiency of a rotor is strongly dependent on the wing section airfoil and blades geometry. At low Reynolds numbers, aerodynamic phenomena such as laminar separation bubbles render the rotor performance highly dependent on the operational conditions. Tab. 1 shows the rotor design parameters and the operational setup adopted in this study.

Table 1. Rotor Design Parameters and Operational Conditions.

Geometry parameters	**Numerical Values**	**Operational Conditions**	
Rotor Diameter, cm	45.00	Angular Speed, RPM	1000
Blade Chord, cm	6.56	–	–
Twist Rate, (°)	-8	–	–
Number of Blades	2	–	–
Solidity(1)	0.1856	–	–

(1) Thrust Weighted Solidity

The rotor design parameters under the operational conditions shown in Tab. 1 were applied in numerical simulations by using an in-house code based on the method Blade Element Momentum. Numerical results are shown in Section 5.

4. Code Validation

Numerical results from our in-house code based on the blade element momentum formulation were compared with experimental data measured by Felker and Mckillip (1994) at the Princeton Dynamic Model Track (Long Track Facility). The testing data were drawn from a 2.44 m diameter rotor composed of four blades linearly twisted (-8°) and shaped with NACA-0015 airfoil. The rotor was tested at a Reynolds numbers based on the wing chord below 250.000. Comparisions between thrust and power coefficients obtained with our in-house code showed a good agreement (with relative errors below 10%) with experimental data from Felker and Mckillip (1994), as well as results from numerical simulations presented by Hernandez (2017) for the same rotor configuration and operational conditions.

5. Numerical Results and Discussion

It is important to understand the effects of geometry parameters on the rotor aerodynamics when developing a conceptual blade design. In viscous flow, the aerodynamic efficiency of a rotor design can be strongly dependent on the operational condition due to the effects of pressure and friction viscous drag and laminar separation bubbles. In this work, the role played by blade taper ratio and twist rate on rotor aerodynamics is assessed for prescribed operational conditions.

Figure 6 shows taper ratio effects on the radial distribution of Reynolds number and relevant aerodynamic parameters

for the rotor design presented in Table 1. According to Figure 6(a), the Reynolds number for taper ratio of 1:1 increases linearly from the blade root toward the tip, since the in-plane linear speed at each blade station is much greater than the induced velocity at 1000 RPM. However, the blade chord narrowing at the tip region reduces the chord-based Reynolds number. Figures 6(b) and 6(c) show the radial distribution of the effective angle of attack for taper ratios of 1:1, 2:1 and 3:1, and thrust coefficients of 0.002 and 0.02, respectively. Regarding the role played by the thrust on the effective angle of attack, there are two main points to be highlighted: the increase in the thrust coefficient leads to a significant increase in the angle of attack and shifts the region of highest angles of attack from the inboard to the mid-span of the blade. However, increasing the blade taper ratio reduces the highest angles of attack, which may delay stall onset.

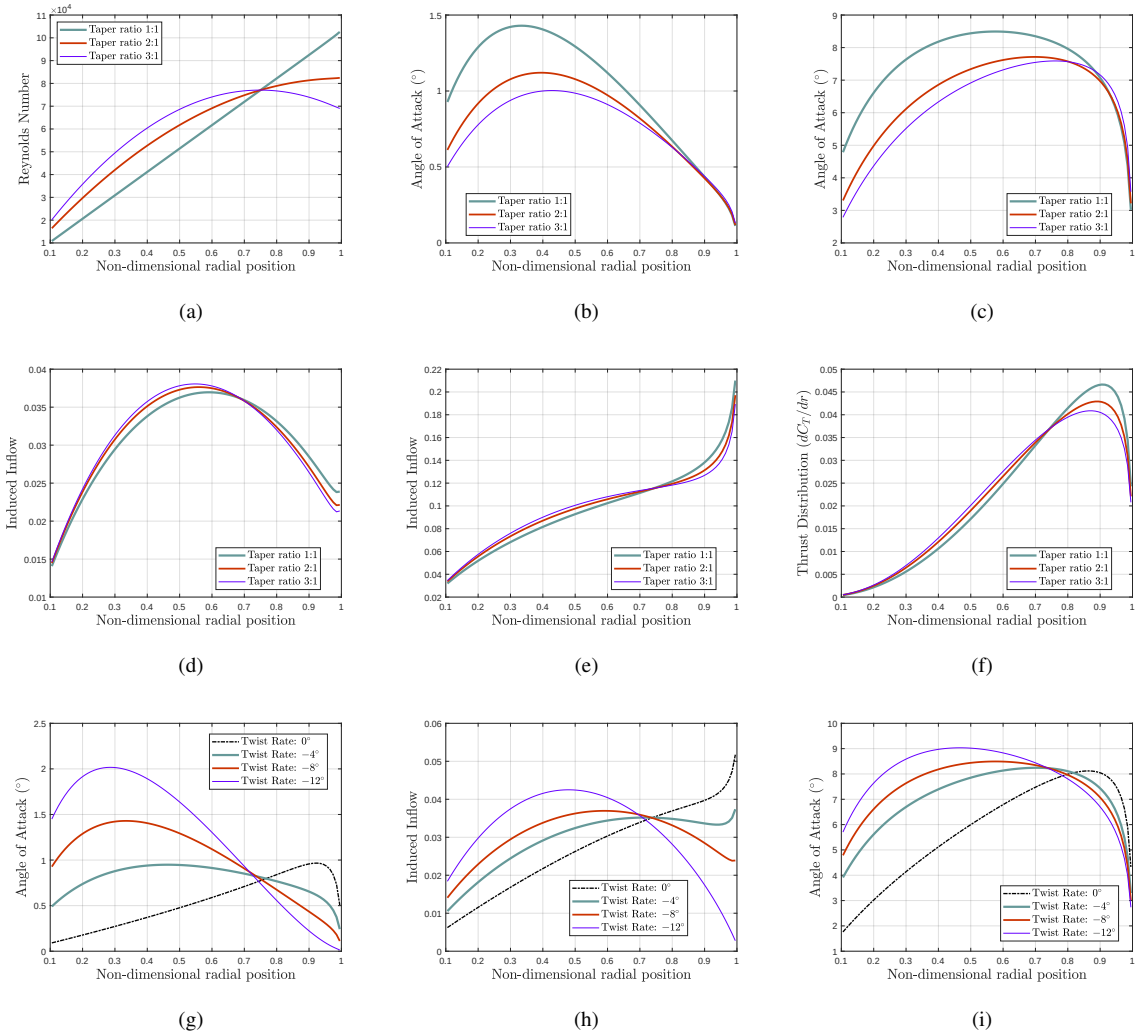

Figure 6. 6(a): spanwise Reynolds number for blades with twist rate of -8° and taper ratios of 1:1, 2:1 and 3:1. 6(b) and 6(c): spanwise angle of attack for blades with twist rate of -8° and taper ratios of 1:1, 2:1 and 3:1. operating at C_T = 0.002 and 0.02, respectively. 6(d) and 6(e) spanwise induced flow for blades with twist rate of -8° and taper ratios of 1:1, 2:1 and 3:1, operating at C_T = 0.002 and 0.02, respectively. 6(f) spanwise thrust gradient for a blade with twist rate of -8° and taper ratios of 1:1, 2:1 and 3:1, operating at C_T = 0.02. 6(g) and 6(h): spanwise distribution of angle of attack and induced flow for untapered blades with twist rate of 0°, -4°, -8°, -12°, operating at C_T = 0.002. 6(i): spanwise distribution of angle of attack and for untapered blades with twist rate of 0°, -4°, -8°, -12°, operating at C_T = 0.02.

.

Figures 6(d) and 6(e) compare spanwise distributions of induced flow, which are very similar for the three taper ratio considered, but vary with the thrust on the rotor disk. Higher levels of induced flow are found at the mid-span region for lower thrust coefficients. For higher thrust coefficients, an overall level increase throughout the blade span is verified, particularly at the blade tip region due an increase in the vortex shedding. Such a three-dimensional effect at the blade tip was taken into account in the numerical model by implementing the Prandtl's tip loss correction. In addition, the more uniform induced flow distribution contributes to reducing the induced power, which potentially increases the rotor efficiency (Leishman, 2006). For C_T = 0.02 (see Figure 6(f)), the spanwise gradient of thrust coefficient reaches the

maximum value at around 90% of the blade span, which is followed by a sharp decrease due to the three-dimensional flow effect caused by the increase of the vortex shedding around the blade tip. Figures 6(g) and 6(i) show the twist rate effects on the radial distribution of the effective angle of attack for an untapered blade operating with thurst coefficients fo C_T = 0.002 and 0.02, respectively. For lower thrusts, the increase in the negative twist rate from moderate values increases the angles of attack at the blade inboard region. According to Figure 6(i), the increase in the thrust coefficient produces an overall increase in the spanwise distribution of effective angle of attack, but a steeper decrease is observed at the blade tip region due to an increase in the induced flow at higher disk loading. Finally, the comparison between Figures 6(g) and 6(h) shows a strong correlation between induced flow and effective angle of attack at low disk loading and within the range of twist rates assessed.

The results presented in Figure 6 are physically consistent and show that the numerical model was able to capture the leading aerodynamic features of a rotary wing operating at hovering flight and low Reynolds, within the range of geometry parameters set to this analysis. Next, a study was conducted to investigate the role played by the blade design on rotor efficiency and required hovering power.

Figure 7(a) shows the Figure of Merit as a function of thrust coefficients set from 0.002 to 0.015, for taper ratios of 1:1, 2:1 and 3:1. As expected, the values of Figure of Merit increase with the thrust coefficient, but no significant effects from taper ratio are observed on the rotor performance. Figure 7(b) shows the rotor Figure of Merit as a function of the blade-loading coefficient (C_T/σ), which takes into account the total blade planform area on the rotor performance. The values of (C_T/σ) were kept below 0.12, which is a representative upper limit to avoid potential stall in contemporary full scale helicopter rotors (Leishman, 2006). As shown in Figure 7(b), blades with greater taper ratios require higher blade-loading coefficients to achieve a target Figure of Merit. The small increase in the rotor efficiency based on the Figure of Merit, when reducing the taper ratio, is consistent with the effect of increasing the blade solidity. It is emphasized here that stall, which limits the rotor efficiency at high thrust, is not considered in the current stage of our numerical simulation. According to Figure 7(c), higher values of power loading are obtained with the untapered blade at lower blade-loading coefficients, whereas tapered blades yield higher values of power loading for higher blade-loading coefficients. It is also interest to note that the blade with highet taper ratio was able to keep the maximum level of power loading within the wider range of non-dimensional blade loading. Figure 6(d) shows that maximum power loading for untapered and twisted blades are achieved at the intermediate range of blade-loading coefficients, even without considering stall effects. Figure 6(e) shows the hover polar plots for all tapered ratios accounted for, from which one concludes that lower hover power is required for the untapered blade at lower blade-loading coefficients. Figure 6(e), in turn, shows very similar hover power curves for all twist rates assessed.

6. Conclusion

This paper presents an ongoing study focused on designing, manufacturing subscale rotary wings and simulating the hover aerodynamic efficiency in hovering flight at low Reynolds numbers. A methodology to design and simulate tapered and twisted blades has been presented and a prototype was built by using the Fused Deposition Modeling (FDM) rapid prototype technique. The aerodynamic efficiency of a tapered and twisted blade shaped with NACA 4412 airfoil was assessed by using a computational code based on the Blade Element Momentum Theory. The numerical simulations were able to capture the effect of blade design parameters on the induced flow field and rotor performance. The initial studies of the CAD drawing, slicing and manufacturing procedures to create accurate subscaled prototypes were proven successful and can be proven useful for future studies on the topic and to start the design of bench tests.

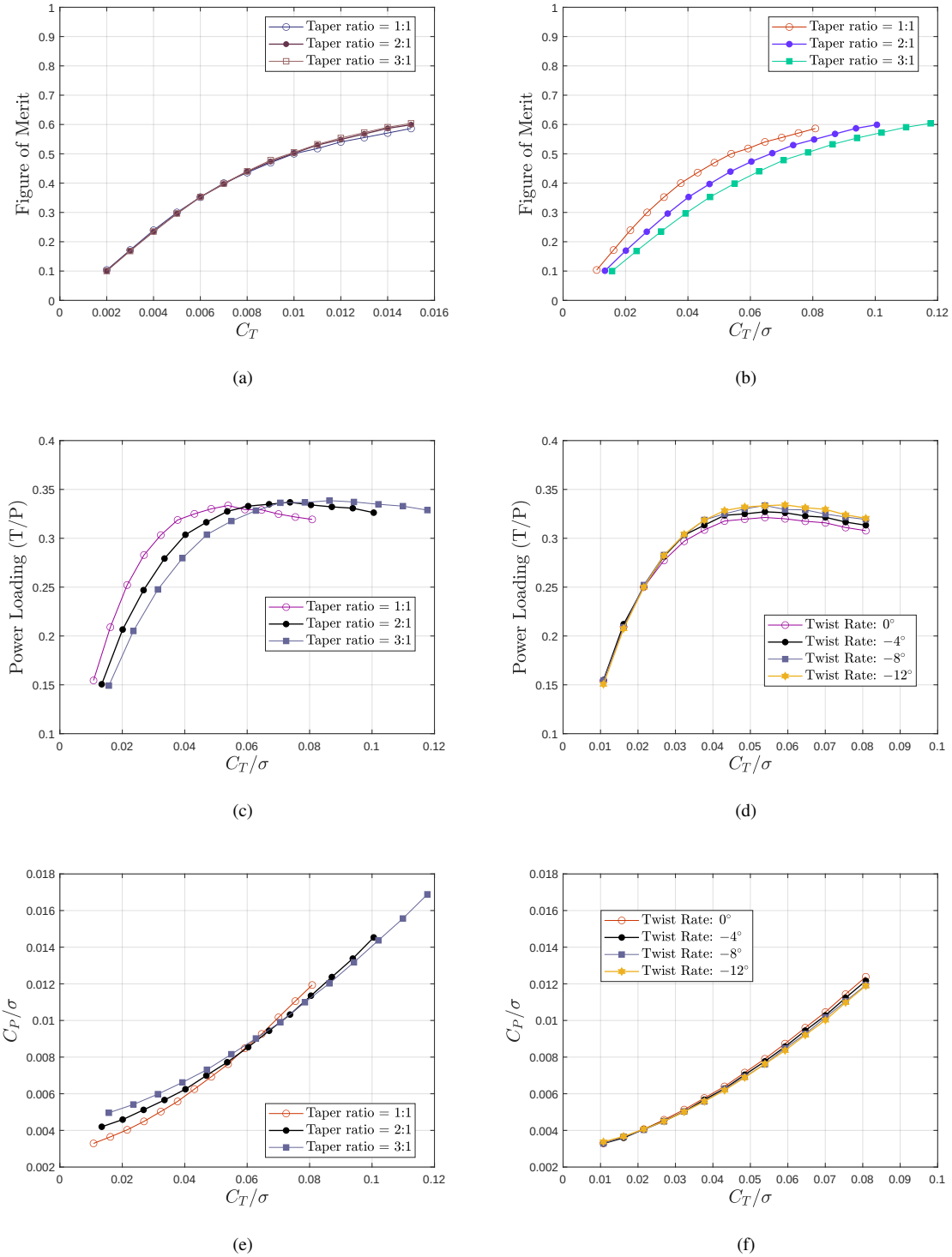

Figure 7. 7(a) and 7(b): Figure of Merit as a function of C_T and C_T/σ, respectively, for blades with twist rate of -8° and taper ratios of 1:1, 2:1 and 3:1. 7(c) power loading as a function of C_T/σ for blades with twist rate of -8° and taper ratios of 1:1, 2:1 and 3:1. 7(d) power loading as a function of C_T/σ for untapered blades with twist rates of 0°, -4°, -8°, -12°. 7(e) hover polar for blades with twist rate of -8° and taper ratios of 1:1, 2:1 and 3:1, and 7(f) hover power for untapered blades with twist rates of 0°, -4°, -8°.

7. REFERENCES

Bohorquez, F., Pines, D. and Samuel, P.D., 2010. "Small rotor design optimization using blade element momentum theory and hover tests". *Journal of Aircraft*, Vol. 47, No. 1, pp. 268–283.

Boni, G.I., Souza, D.S. and Pagani, C.C., 2021. "A numerical study of rotor hover performance at low reynolds number flow". In *Proceedings of the 26nd International Congress of Mechanical Engineering - COBEM 2021*. Virtual Congress, Brazil.

Casalino, D., Grande, E., Romani, G., Ragni, D. and Avallone, F., 2021. "Definition of a benchmark for low reynolds number propeller aeroacoustics". *Aerospace Science and Technology*, Vol. 113.

Clausen, P., Evans, S. and Wood, D., 2023. "Design, manufacture, and testing of small wind turbine blades". In P. Brøndsted, R. Nijssen and S. Goutianos, eds., *Advances in Wind Turbine Blade Design and Materials (Second Edition)*, Woodhead Publishing, Woodhead Publishing Series in Energy, pp. 441–461.

Leishman, J.G., 2006. *Principles of Helicopter Aerodynamics*. 2nd edn. New York. Cambridge Univeristy Press.

Loureiro, E.V., Oliveira, N.L., Hallaka, P.H., Bastosa, F.S., Rochab, L.M., Delmontec, R.G. and Lemonge, A.C.C., 2021. "Evaluation of low fidelity and cfd methods for the aerodynamic performance of a small propeller". *Aerospace Science and Technology*, Vol. 108.

Muller, T.J. and Delaurier, J.D., 2003. "Aerdynamics of small veiches". *Annual Review of Fluid Mechanics*, Vol. 35, p. 89111.

Schiller, G.L., 2015. "Additive manufacturing for aerospace". In *2015 IEEE Aerospace Conference*. IEEE, Big Sky, MT, USA.

Seddon, J.M. and Newman, S., 2011. *Basic Helicopter Aerodynamics*. Willey.

Sun, H. and Lee, S., 2005. "Response surface approach to aerodynamic optimization design of helicopter rotor blade". *International Journal for Numerical Methods in Engineering*, Vol. 64.

Valavanis, K.P. and Vachtsevanos, G.J., 2014. *Handbook of Unmanned Aerial Vehicles*. Springer Publishing Company, Incorporated. ISBN 9048197066.

8. RESPONSIBILITY NOTICE

The authors are solely responsible for the printed material included in this paper.